Rapid Communications

Balanced electron-hole transport in spin-orbit semimetal $SrIrO_3$ heterostructures

Nicola Manca,[1,*] Dirk J. Groenendijk,[1] Ilaria Pallecchi,[2] Carmine Autieri,[3] Lucas M. K. Tang,[4] Francesca Telesio,[5] Giordano Mattoni,[1] Alix McCollam,[4] Silvia Picozzi,[3] and Andrea D. Caviglia[1]

[1]*Kavli Institute of Nanoscience, Delft University of Technology, P.O. Box 5046, 2600 GA Delft, The Netherlands*
[2]*CNR-SPIN, c/o Dipartimento di Fisica, University of Genoa, Via Dodecaneso 33, 16146 Genova, Italy*
[3]*Consiglio Nazionale delle Ricerche CNR-SPIN, UOS L'Aquila, Sede Temporanea di Chieti, 66100 Chieti, Italy*
[4]*High Field Magnet Laboratory (HFML-EMFL), Radboud University, Toernooiveld 7, 6525 ED, Nijmegen, The Netherlands*
[5]*Dipartimento di Fisica, University of Genoa, Via Dodecaneso 33, 16146 Genova, Italy*

(Received 14 November 2017; published 13 February 2018; corrected 4 September 2019)

Relating the band structure of correlated semimetals to their transport properties is a complex and often open issue. The partial occupation of numerous electron and hole bands can result in properties that are seemingly in contrast with one another, complicating the extraction of the transport coefficients of different bands. The 5*d* oxide $SrIrO_3$ hosts parabolic bands of heavy holes and light electrons in gapped Dirac cones due to the interplay between electron-electron interactions and spin-orbit coupling. We present a multifold approach relying on different experimental techniques and theoretical calculations to disentangle its complex electronic properties. By combining magnetotransport and thermoelectric measurements in a field-effect geometry with first-principles calculations, we quantitatively determine the transport coefficients of different conduction channels. Despite their different dispersion relationships, electrons and holes are found to have strikingly similar transport coefficients, yielding a holelike response under field-effect and thermoelectric measurements and a linear electronlike Hall effect up to 33 T.

DOI: 10.1103/PhysRevB.97.081105

Oxide heterostructures have been intensely studied in recent years as a versatile platform for controlling electronic properties of materials [1]. Charge transfer, strain engineering, and polar instabilities are part of the toolbox available at oxide interfaces for controlling phases of matter, such as two-dimensional superconductors and various magnetic ground states. Although the manipulation of broken symmetries is a well-developed topic in the field, experimental control of topological phases at oxide interfaces has so far been elusive. Symmetry-protected boundary states in oxide heterostructures have been considered theoretically as a promising route to realize novel topological materials. Much attention has been focused on $SrIrO_3$ and its heterostructures as candidates for correlated topological insulators [2,3], topological semimetals [4,5], topological Hall effect [6], and unconventional superconductors [7–9]. In its bulk form this material exhibits a nodal line at the U point and characteristic transport signatures of Dirac electrons, such as large and linear magnetoresistances [10–12]. However, when synthesised as an epitaxial thin film, $SrIrO_3$ shows transport characteristics that are inconsistent with this picture and not yet understood, including a linear and strongly reduced magnetoresistance [13,14]. Angle-resolved photoemission spectroscopy shows that the degeneracy at the Dirac points is lifted, leading to a Fermi surface with pockets of light electrons together with heavy holes [15,16]. X-ray diffraction studies have correlated this modification of the electronic structure to an epitaxially stabilized lattice distortion that breaks the orthorhombic bulk symmetry [17,18]. An understanding of the charge and transport properties of this correlated semimetal is a fundamental step for the realization of topological phases in oxide heterostructures and is developed here.

Here, we report on an extensive characterization of the transport properties of heteroepitaxial $SrIrO_3/SrTiO_3$ by combined field-effect, magnetotransport, and thermoelectric measurements. Numerical analysis, supported by first-principles calculations, account for the coexistence of an electronlike Hall effect with a holelike electrical conductivity and thermopower. The emerging picture of a compensated semimetallic state harmonizes transport and spectroscopic data.

$SrIrO_3$ thin films were grown by pulsed laser deposition on single-crystal $SrTiO_3$[001] substrates and then encapsulated *in situ* with a $SrTiO_3$ layer to prevent degradation during lithographic processing [19]. Details of growth conditions and sample characterization of $SrIrO_3/SrTiO_3$ heterostructures are discussed in Ref. [19]. Magnetotransport measurements were acquired in a four-probe configuration in a flow cryostat with a base temperature of 1.6 K. The Seebeck effect was measured in a physical properties measurement system by Quantum Design equipped with thermal transport option in the continuous scanning mode with a 0.4-K/min cooling rate. First-principles density functional theory calculations were performed within the generalized gradient approximation (GGA) by using the plane-wave VASP [20] package and the PBEsol for the exchange-correlation functional [21] with spin-orbit coupling. The Hubbard U effects on the Ir sites were included within the GGA + U [22] approach using the rotational invariant scheme [23]. With U larger than 1 eV, the bulk is magnetic. To deal with the nonmagnetic bulk Ir compounds [24], we assumed $U = 0.80$ eV and $J_H = 0.15U$. The core and the valence electrons were treated with the projector augmented-wave method [25], and a cutoff of

*nicola.manca@spin.cnr.it

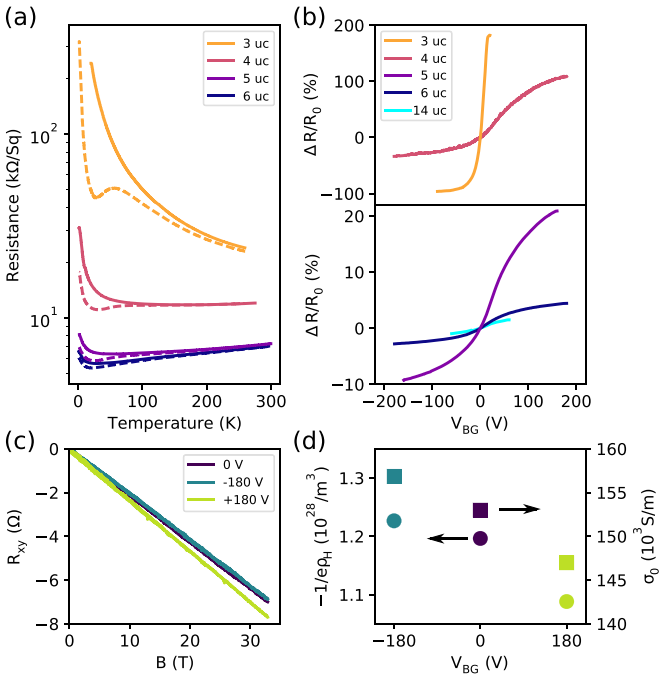

FIG. 1. Magnetotransport under field effects in $SrIrO_3$ thin films. (a) $R(T)$ for different thicknesses measured at $V_{BG} = 0$ V (the solid lines) and $V_{BG} = -180$ V (the dashed lines). (b) Relative variation of the electrical resistance at 1.6 K vs V_{BG}, both metallic and semiconducting samples show the same qualitative response. (c) Hall resistance of a six-unit-cell (uc) thin film for different V_{BG}'s at 1.6 K. (d) Free-electron density calculated from (d) in a single band picture (circles) and $\sigma_0(V_{BG})$ (the squares).

400 eV for the plane-wave basis was used. An $8\times8\times6$ k-point Monkhorst-Pack grid [26] was used for the calculation of the bulk phase.

Figure 1(a) shows resistance vs temperature [$R(T)$] characteristics of $SrIrO_3$ films of different thicknesses (the solid lines). As recently reported, a metal-insulator transition occurs between four and three ucs and bulklike electrical resistivity is reached above six ucs [27,28]. Through the application of a back-gate voltage (V_{BG}), the carrier density of the $SrIrO_3$ films can be tuned by the field effect. This technique is often used in low-density two-dimensional systems or semiconductors to change the carrier density and consequently the resistance. The dashed $R(T)$ curves in Fig. 1(a) show a huge resistance change upon the application of $V_{BG} = -180$ V, indicative of the low carrier density of this system. The field-effect efficiency decreases with the thickness and above six ucs the $R(T)$ plots measured with $V_{BG} = 0$ and $V_{BG} = -180$ V are not distinguishable. The way the electric field affects the $R(T)$ characteristics gives us a first hint of the carrier type of the system: A negative V_{BG} lowers the resistance as expected from a conductor whose carriers are holes. Figure 1(b) shows the relative variation of the electrical resistance, measured on samples of different thicknesses while sweeping V_{BG} at 1.6 K. The holelike response is consistent over the whole range of thicknesses explored, independent of the semiconducting or metallic behavior [27]. Reducing the $SrIrO_3$ thickness the gating efficiency becomes more pronounced because of the decreased screening effect from the free carriers, and for the three-uc case we can even reach an insulating state by the field effect [Fig. 1(b)]. At base temperature it is possible to observe a field effect even for thicknesses above six ucs, and in Fig. 1(b) we show the 14-uc case (cyan plot) where, as expected from the strong screening effect, the signal is very small, on the order of a few percent. We note that the response to the back gate is mediated by the dielectric constant of the $SrTiO_3$ substrate (ε_r^{STO}). The nonlinear temperature and electric-field dependence of ε_r^{STO} determine the nonmonotonic behavior of the $R(T)$'s with applied V_{BG} in Fig. 1(a) and the reduced gating efficiency at high voltages observed in Fig. 1(b) [29,30]. In the Supplemental Material, Sec. I we provide further evidence of a hole-dominated electrical conductivity (σ_0), showing the effect of doping $SrIrO_3$ thin films with oxygen vacancies [31].

Previous literature reports showed that the Hall effect in $SrIrO_3$ thin films is negative and almost linear [14], which is at odds with the hole-type field-effect response. To study this, we choose a thickness of six ucs, which is small enough to be tunable by a field effect and large enough to be sufficiently conductive at low temperatures. The corresponding Hall effect measured at 1.6 K is presented in Fig. 1(c). It is linear and negative up to 33 T, similar to what would be observed in a system dominated by a single band of electrons. However, the response of the Hall signal (ρ_H) and conductivity at zero magnetic field (σ_0) to the V_{BG}, reported in Fig. 1(d), show that such a simple picture is inadequate. Despite its negative slope, the Hall signal responds to the back gate as if the electrical transport is dominated by hole carriers. Furthermore, the carrier density calculated in a single band picture ($1/\rho_H \approx 10^{28}$ m^{-3}) would make the back gate almost ineffective because of the strong screening effect. The discrepancy between Hall and field-effect data is a clear indication of the multiband character of this system.

The Hall resistivity of two parallel channels of holes and electrons is given by

$$\rho_H \equiv \frac{tR_{xy}}{B} = \frac{1}{e}\frac{n_h\mu_h^2 - n_e\mu_e^2 + (n_h - n_e)(\mu_h\mu_e B)^2}{\sigma_0^2/e^2 + (n_h - n_e)^2(\mu_h\mu_e B)^2}, \quad (1)$$

where

$$\sigma_0 = \sigma_h + \sigma_e = e(n_h\mu_h + n_e\mu_e), \quad (2)$$

and t is the film thickness, R_{xy} is the Hall resistance, e is the elementary charge, B is the magnetic field, n is the carrier density, μ is the mobility, and e and h indicate electrons and holes, respectively. Since the measured Hall effect from Fig. 1(c) is linear and negative we can approximate Eq. (1) with its low-field limit,

$$\rho_H = \frac{e}{\sigma_0^2}\left(n_h\mu_h^2 - n_e\mu_e^2\right). \quad (3)$$

Standard analysis on two-band systems is based on the combined measurement of σ_0 and ρ_{xy} where the presence of flex points in the magnetic-field dependence of ρ_{xy} provides a powerful constraint for the calculation of carrier densities and mobilities of the conduction channels. Because in our case such flex points are likely out of the probed range (±33 T), the extraction of the carrier parameters in $SrIrO_3$ thin films remains undetermined.

Thermoelectric measurements can provide complementary information to magnetotransport, allowing us to identify the transport coefficients of the two carriers. For this experiment

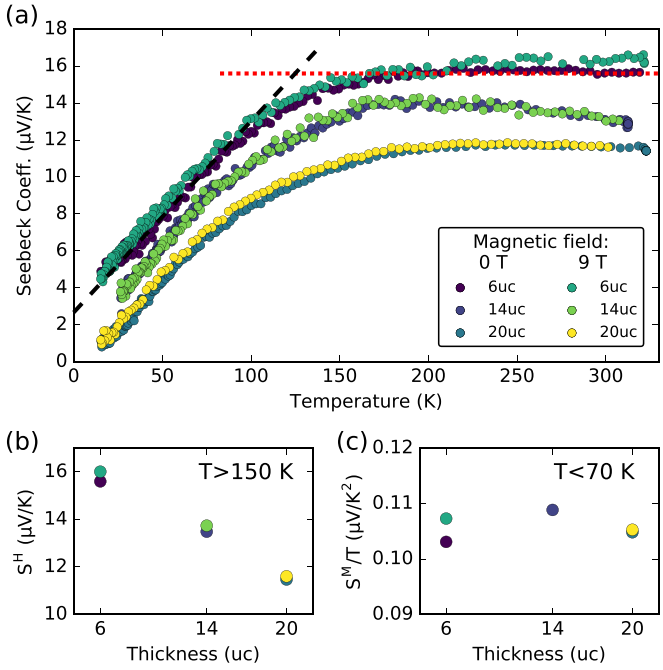

FIG. 2. Thermoelectric measurements on $SrIrO_3$ thin films. (a) Seebeck coefficient as a function of temperature, thickness, and magnetic field. (b) Seebeck coefficient corresponding to Eq. (4) and (c) Seebeck slope used in Eq. (5). The lines in (a) show a linear fit used to extract the data in (b) (red dotted line) and (c) (black dashed line), corresponding to the high (>150-K) and and low (<70-K) temperature regimes.

we prepared a dedicated series of samples having sizes of 10×5 mm^2 and thicknesses of six, 14, and 20 ucs. Samples thinner than six ucs were not measurable because of the high noise at the electrical contacts, in particular at low temperatures. We thus measured the Seebeck coefficient (S) of metallic $SrIrO_3$ films as a function of thickness, temperature, and magnetic field. The experimental results are presented in Fig. 2(a) where all the samples show a nearly constant positive value of $S \approx 10$–20 μV/K above 150 K and a linear decrease below 70 K. As opposed to what is observed in bulk $SrIrO_3$ samples [32], here the Seebeck coefficient does not show multiple sign changes, indicating a drastically different electronic structure. A further difference is the absence of any magnetic-field dependence of the thermoelectric response, indicating that in thin films the Seebeck effect is dominated by the diffusive mechanism. The high (>150-K) and low (<70-K) temperature regimes are well described by the formulas of Heikes [33] and Mott [34], respectively, which provide a direct relationship between the measured quantities and the microscopic material properties. For each single band of either holes or electrons, the formulas of Heikes *et al.* [33] (S^{H}) and Mott (S^{M}) Seebeck coefficients are as follows:

$$S^{\mathrm{H}}_{\mathrm{h/e}} = \pm\frac{k_{\mathrm{B}}}{e}\log\left(\frac{2-n\nu}{n\nu}\right), \tag{4}$$

$$S^{\mathrm{M}}_{\mathrm{h/e}} = \pm\left(\frac{3}{2}-\alpha\right)\left(\frac{2(2\pi)^8}{3^5}\right)^{1/3}\frac{k_{\mathrm{B}}^2}{e\hbar^2}\frac{m^*}{n^{2/3}}T, \tag{5}$$

where k_{B} is the Boltzmann constant, $\hbar$ is the reduced Planck constant, ν is the unit-cell volume, α is a parameter related

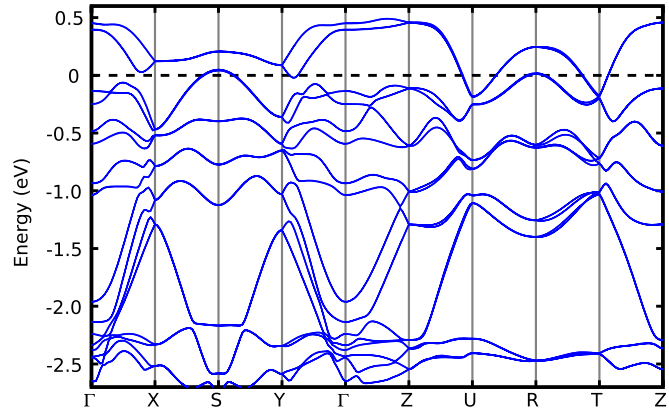

FIG. 3. Electronic band structure of bulk $SrIrO_3$ at $U = 0.80$ eV with lattice constants $a = 3.905$ Å and $c = 4.08$ Å.

to the scattering mechanisms ($0 \leqslant \alpha \leqslant 1$), m^* is the effective mass of the carriers, and the $\pm$ sign corresponds to holes or electrons, respectively. In a multiband picture the total Seebeck coefficient in diffusive regime can be expressed as

$$S = \frac{e}{\sigma_0}(n_{\mathrm{h}}\mu_{\mathrm{h}}|S_{\mathrm{h}}| - n_{\mathrm{e}}\mu_{\mathrm{e}}|S_{\mathrm{e}}|). \tag{6}$$

That in combination with Eqs. (4) and (5) allows us to write the Seebeck coefficient in the two temperature regimes,

$$S^{\mathrm{H}} = \frac{k_{\mathrm{B}}}{\sigma_0}\left[n_{\mathrm{h}}\mu_{\mathrm{h}}\log\left(\frac{2-n_{\mathrm{h}}\nu}{n_{\mathrm{h}}\nu}\right) - n_{\mathrm{e}}\mu_{\mathrm{e}}\log\left(\frac{2-n_{\mathrm{e}}\nu}{n_{\mathrm{e}}\nu}\right)\right], \tag{7}$$

$$S^{\mathrm{M}} = \frac{e}{\sigma_0}\xi\left(n_{\mathrm{h}}^{1/3}\mu_{\mathrm{h}}m_{\mathrm{h}}^* - n_{\mathrm{e}}^{1/3}\mu_{\mathrm{e}}m_{\mathrm{e}}^*\right)T, \tag{8}$$

where ξ is the numerical prefactor appearing in Eq. (5),

$$\xi = \left(\frac{3}{2}-\alpha\right)\left(\frac{2(2\pi)^8}{3^5}\right)^{1/3}\frac{k_{\mathrm{B}}^2}{e\hbar^2}.$$

The experimental values for S^{H} and S^{M}/T are presented in Figs. 2(b) and 2(c) as a function of the film thickness, where S^{H} is calculated as the average of S above 150 K and S^{M}/T is determined from linear fitting of S below 70 K. Although the thermoelectric response at low-temperature S^{M}/T does not show any thickness dependence at high-temperature S^{H} decreases linearly with the thickness. This could be an indication of a different balance of electrons and holes when approaching the metal-insulator transition [27].

The analysis of the thermoelectric response relies on fixing the values of the free parameters of Eq. (8) (α,m_{e}^*,m_{h}^*) on the basis of theoretical considerations. Here, $\alpha = 0.5$ was used, which is the typical choice when scattering is dominated by impurities or phonons [35]. To estimate the effective masses in $SrIrO_3$ thin films, we study the electronic structure of $SrIrO_3$

TABLE I. Input parameters of the sampling algorithm.

t (uc)	ρ_{H} (nΩ m T^{-1})	σ_0 (S/m)	S^{H} (μV/K)	S^{M} (nV/K^2)
30	−1.27	1.0×10^5	12 ± 1	105 ± 5
6	−0.45	1.5×10^5	16 ± 1	105 ± 5

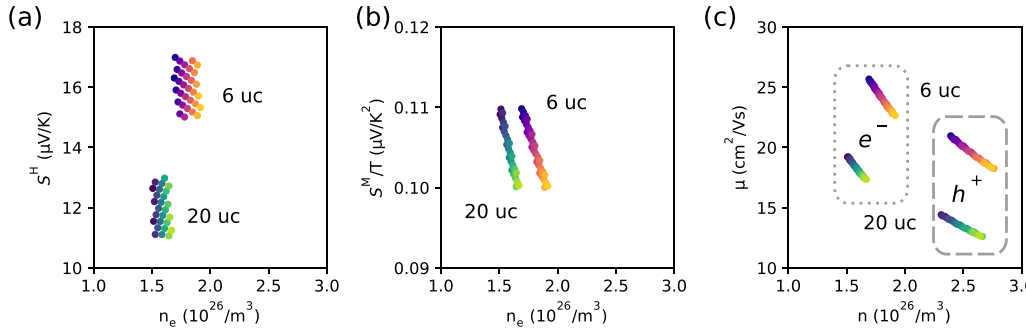

FIG. 4. Transport coefficients of 20- and 6-uc $SrIrO_3$ thin films. (a) Total Seebeck coefficients from the formulas of Heikes [33] and (b) Mott of acceptable $\{n_i,\mu_i\}$ combinations. Here, only electrons are shown for clarity. (c) Free-carrier densities and mobilities for electrons (points) and holes (the dashed lines) satisfying the experimental constraints.

in the thick-film limit by means of first-principles calculations. The in-plane lattice parameters was fixed to the value of the $SrTiO_3$ substrate (3.905 Å), and the out-of-plane lattice parameter was fixed to the experimental value for $SrIrO_3$ (4.08 Å) [19]. Figure 3 shows the corresponding band structure where the density of states near the Fermi level is dominated by the $5d$ t_{2g} contribution as in orthorhombic bulk $SrIrO_3$. We calculate the effective masses for the holes at the maxima of the dispersion relations close to the Fermi level located at the S and R points and find an average value of $m_h^* = 1.55m_e$. At the U and T points and along the Y-Γ directions, we have the minima, and the corresponding average effective mass from the electron is $m_e^* = 0.34m_e$. These values are in agreement with the effective masses extracted from angle-resolved photoemission spectroscopy measurements performed on $SrIrO_3/SrTiO_3$ heterostructures [16].

In the following, we evaluate n_e, μ_e, n_h, and μ_h by using a direct sampling algorithm. Equations (2), (3), (7), and (8) are linearly independent and can therefore be combined to determine n_i and μ_i. For each combination of (n_e,μ_e) the corresponding (n_h,μ_h) pair is calculated by using the experimental σ_0 and ρ_H in Eqs. (2) and (3). The resulting (n_i,μ_i) set is accepted if the Hall effect calculated with Eq. (1) and the thermoelectric coefficients S^H and S^M/T, calculated with Eqs. (7) and (8), agree with the experimental data (see also the Supplemental Material, Sec. II for further details [31]). Table I shows the experimental values used as input parameters where the ± on the Seebeck coefficients indicates the range of the acceptance condition. Since the values of ρ_H and σ_0 above 15 ucs show no thickness dependence [27], we combine electrical transport data from a thick (30-uc) sample with the 20-uc Seebeck data to perform the analysis. The calculated (n_i,μ_i) combinations for both 20 and 6 ucs are presented in Figs. 4(a) and 4(b), whereas Fig. 4(c) shows the corresponding transport coefficients. Each (n_i,μ_i) set is a possible solution satisfying the experimental constraints, and multiple sets are accepted because of the tolerances reported in Table I. We find that the carrier density and mobility for electrons and holes must be located in two closely spaced groups of points on the (n,μ) plane with the electrons having higher mobility and lower density than the holes. Table II reports the centers of these groups together with the corresponding conductance of each channel. The ratio between electron and hole carrier densities is not dramatic (≈1.7), confirming the marked multiband character of this system. The results from this analysis are consistent with the experimental observation of a hole-dominated electrical conductivity ($\sigma_h > \sigma_e$), although this constraint was not explicitly introduced into the analysis. This is in agreement with both back-gate experiments presented in Fig. 1 and the oxygen vacancies doping experiment reported in the Supplemental Material, Sec. I [31]. The calculated n_e's are two orders of magnitude lower than that obtained in a single band picture, showing that the measured Hall signals are determined by carrier compensation. These values have a weak temperature dependence since both ρ_H and σ_0 show small temperature variations [27] and the Seebeck coefficients at low and high temperatures are in good agreement with Eqs. (4) and (5). From the results of Table II it is possible to calculate the cyclotron component of the magnetoresistance and compare it with the measured one. This is discussed in the Supplemental Material, Sec. III [31] where we show that our analysis is compatible with the experimental data in the framework of the present literature [36–43].

In conclusion, we investigated the electronic structure of $SrIrO_3$ thin films by means of multiple transport techniques. The semimetallic nature of $SrIrO_3$ manifests itself in a Hall effect dominated by electrons and a holelike electrical conductivity and Seebeck effect. The combination of magnetotransport and thermoelectric measurements with first-principles calculations allows for obtaining a limited ensemble of possible transport coefficients for the charge carriers. Our results indicates that electrons and holes have similar densities and mobilities, yet the higher conductivity of the hole channel makes it dominant in the electrical transport. This analysis

TABLE II. Charge-carrier characteristics extracted from the sampling analysis with the experimental constraints.

t (uc)	n_e (10^{26}/cm^3)	n_h (10^{26}/cm^3)	μ_e (cm^2 V^{-1} s^{-1})	μ_h (cm^2 V^{-1} s^{-1})	σ_e (S/m)	σ_h (S/m)
20	1.6	2.5	18	13.5	4.6	5.4
6	1.8	2.6	27	22	7.8	9.1

constitutes a comprehensive and robust description of the electronic structure of $SrIrO_3$, paving the way for future studies on $SrIrO_3$-based heterostructures and that can be extended to unravel the electronic structure of other semimetallic compounds.

This Rapid Communication was supported by The Netherlands Organisation for Scientific Research (NWO/OCW) as part of the Frontiers of Nanoscience Program (NanoFront), by the Dutch Foundation for Fundamental Research on Matter (FOM), and by CNR-SPIN via the Seed Project "CAMEO."

[1] P. Zubko, S. Gariglio, M. Gabay, P. Ghosez, and J.-M. Triscone, Annu. Rev. Condens. Matter Phys. **2**, 141 (2011).
[2] D. Pesin and L. Balents, Nat. Phys. **6**, 376 (2010).
[3] M. Kargarian, J. Wen, and G. A. Fiete, Phys. Rev. B **83**, 165112 (2011).
[4] B.-J. Yang and N. Nagaosa, Phys. Rev. Lett. **112**, 246402 (2014).
[5] Y. Chen, Y.-M. M. Lu, and H.-Y. Y. Kee, Nat. Commun. **6**, 6593 (2015).
[6] J. Matsuno, K. Ihara, S. Yamamura, H. Wadati, K. Ishii, V. V. Shankar, H.-Y. Kee, and H. Takagi, Phys. Rev. Lett. **114**, 247209 (2015).
[7] F. Wang and T. Senthil, Phys. Rev. Lett. **106**, 136402 (2011).
[8] J. Kim, D. Casa, M. H. Upton, T. Gog, Y.-J. Kim, J. F. Mitchell, M. van Veenendaal, M. Daghofer, J. van den Brink, G. Khaliullin, and B. J. Kim, Phys. Rev. Lett. **108**, 177003 (2012).
[9] Z. Y. Meng, Y. B. Kim, and H.-Y. Kee, Phys. Rev. Lett. **113**, 177003 (2014).
[10] J.-M. Carter, V. V. Shankar, M. A. Zeb, and H.-Y. Kee, Phys. Rev. B **85**, 115105 (2012).
[11] M. A. Zeb and H.-Y. Kee, Phys. Rev. B **86**, 085149 (2012).
[12] J. Fujioka, T. Okawa, A. Yamamoto, and Y. Tokura, Phys. Rev. B **95**, 121102 (2017).
[13] A. Biswas, K. S. Kim, and Y. H. Jeong, J. Appl. Phys. **116**, 213704 (2014).
[14] L. Zhang, Q. Liang, Y. Xiong, B. Zhang, L. Gao, H. Li, Y. B. Chen, J. Zhou, S.-T. Zhang, Z.-B. Gu, S.-h. Yao, Z. Wang, Y. Lin, and Y.-F. Chen, Phys. Rev. B **91**, 035110 (2015).
[15] Y. F. Nie, P. D. C. King, C. H. Kim, M. Uchida, H. I. Wei, B. D. Faeth, J. P. Ruf, J. P. C. Ruff, L. Xie, X. Pan, C. J. Fennie, D. G. Schlom, and K. M. Shen, Phys. Rev. Lett. **114**, 016401 (2015).
[16] Z. T. Liu, M. Y. Li, Q. F. Li, J. S. Liu, W. Li, H. F. Yang, Q. Yao, C. C. Fan, X. G. Wan, Z. Wang, and D. W. Shen, Sci. Rep. **6**, 30309 (2016).
[17] J. Liu, D. Kriegner, L. Horak, D. Puggioni, C. Rayan Serrao, R. Chen, D. Yi, C. Frontera, V. Holy, A. Vishwanath, J. M. Rondinelli, X. Marti, and R. Ramesh, Phys. Rev. B **93**, 085118 (2016).
[18] L. Horák, D. Kriegner, J. Liu, C. Frontera, X. Marti, and V. Holý, J. Appl. Crystallogr. **50**, 1 (2017).
[19] D. J. Groenendijk, N. Manca, G. Mattoni, L. Kootstra, S. Gariglio, Y. Huang, E. van Heumen, and A. D. Caviglia, Appl. Phys. Lett. **109**, 041906 (2016).
[20] G. Kresse and D. Joubert, Phys. Rev. B **59**, 1758 (1999).
[21] J. P. Perdew, A. Ruzsinszky, G. I. Csonka, O. A. Vydrov, G. E. Scuseria, L. A. Constantin, X. Zhou, and K. Burke, Phys. Rev. Lett. **100**, 136406 (2008).
[22] V. I. Anisimov, J. Zaanen, and O. K. Andersen, Phys. Rev. B **44**, 943 (1991).
[23] A. I. Liechtenstein, V. I. Anisimov, and J. Zaanen, Phys. Rev. B **52**, 5467(R) (1995).
[24] B. Kim, P. Liu, and C. Franchini, Phys. Rev. B **95**, 115111 (2017).
[25] P. E. Blöchl, Phys. Rev. B **50**, 17953 (1994).
[26] J. D. Pack and H. J. Monkhorst, Phys. Rev. B **16**, 1748 (1977).
[27] D. J. Groenendijk, C. Autieri, J. Girovsky, M. C. Martinez-Velarte, N. Manca, G. Mattoni, A. M. R. V. L. Monteiro, N. Gauquelin, J. Verbeeck, A. F. Otte, M. Gabay, S. Picozzi, and A. D. Caviglia, Phys. Rev. Lett. **119**, 256403 (2017).
[28] P. Schütz, D. Di Sante, L. Dudy, J. Gabel, M. Stübinger, M. Kamp, Y. Huang, M. Capone, M.-A. A. Husanu, V. N. Strocov, G. Sangiovanni, M. Sing, and R. Claessen, Phys. Rev. Lett. **119**, 256404 (2017).
[29] R. C. Neville, B. Hoeneisen, and C. A. Mead, J. Appl. Phys. **43**, 2124 (1972).
[30] D. Davidovikj, N. Manca, H. S. J. van der Zant, A. D. Caviglia, and G. A. Steele, Phys. Rev. B **95**, 214513 (2017).
[31] See Supplemental Material at http://link.aps.org/supplemental/10.1103/PhysRevB.97.081105 for the effect of oxygen vacancies doping, details of the sampling algorithm, and the analysis of the magnetoresistance.
[32] I. Pallecchi, M. T. Buscaglia, V. Buscaglia, E. Gilioli, G. Lamura, F. Telesio, M. R. Cimberle, and D. Marré, J. Phys.: Condens. Matter **28**, 065601 (2016).
[33] R. Heikes, R. Miller, and R. Mazelsky, Physica **30**, 1600 (1964).
[34] M. Jonson and G. D. Mahan, Phys. Rev. B **21**, 4223 (1980).
[35] I. Pallecchi, M. Codda, E. Galleani d'Agliano, D. Marré, A. D. Caviglia, N. Reyren, S. Gariglio, and J.-M. Triscone, Phys. Rev. B **81**, 085414 (2010).
[36] A. A. Abrikosov, Phys. Rev. B **58**, 2788 (1998).
[37] M. M. Parish and P. B. Littlewood, Nature (London) **426**, 162 (2003).
[38] M. M. Parish and P. B. Littlewood, Phys. Rev. B **72**, 094417 (2005).
[39] A. Gerber, I. Kishon, I. Y. Korenblit, O. Riss, A. Segal, M. Karpovski, and B. Raquet, Phys. Rev. Lett. **99**, 027201 (2007).
[40] J. Hu and T. F. Rosenbaum, Nat. Mater. **7**, 697 (2008).
[41] K. K. Huynh, Y. Tanabe, and K. Tanigaki, Phys. Rev. Lett. **106**, 217004 (2011).
[42] N. Kozlova, N. Mori, O. Makarovsky, L. Eaves, Q. Zhuang, A. Krier, and A. Patanè, Nat. Commun. **3**, 1097 (2012).
[43] P. S. Alekseev, A. P. Dmitriev, I. V. Gornyi, V. Y. Kachorovskii, B. N. Narozhny, M. Schütt, and M. Titov, Phys. Rev. Lett. **114**, 156601 (2015).

Correction: The caption to Fig. 1 contained a typographical error and has been fixed. Table II contained errors with the powers of 10 and has been fixed.